"This Town Ain't Big Enough for the Both of Us": But how big would be big enough? Can it be too big?

Tony H. Kim

1 Preliminaries

In this assignment we investigate the law of competitive exclusion. Stated in 1934 by G.F. Gause, competitive exclusion states that two competing species can coexist only if they exploit their environment differently. Our laboratory is the following dynamical system in N_1, N_2 and P:

$$\dot{N_1} = N_1 \cdot (r - \frac{r}{k}N_1 - \frac{r}{k}N_2 - bP) \tag{1}$$

$$\dot{N_2} = N_2 \cdot (r - \frac{r}{k}\alpha N_1 - \frac{r}{k}N_2 - (b-\epsilon)P) \tag{2}$$

$$\dot{P} = P \cdot (cbN_1 + c(b-\epsilon)N_2 - d) \tag{3}$$

where N_1 and N_2 represent the two prey populations, and P the population of the predator. A brief discussion of the parameters $(r, k, \alpha, b, \epsilon, c, d)$ follows:

Clearly, the parameter $r > 0$ signifies the growth rate of the prey populations as evidenced by the linear growth terms $\dot{N_i} = rN_i$. The significance of the parameter $k > 0$ can be easily inferred by rewriting the equation in $\dot{N_1}$ as:

$$\dot{N_1} = N_1 \cdot (r - \frac{r}{k} \cdot (N_1 + N_2) - bP) \tag{4}$$

where it is evident that, in the absence of the predator, if $N_1 + N_2 = k$ then $\dot{N_1} = 0$. Hence, we may interpret the parameter k as the natural "carrying capacity" for the prey populations. As hinted by the title, the focus of this study is to observe the effects of k on the dynamics of the (N_1, N_2, P) system.

In the above manner we also interpret the parameter $\alpha \geq 1$. We see that $\dot{N_2} = 0$ when the term $\alpha N_1 + N_2$ equals k. However, since the parameter α magnifies the "effective" population of N_1 in smothering the growth of N_2, α gives a measure of the inherent advantage that N_1 has over N_2.

The coefficient b in the overlap terms N_iP gives the rate at which N_i are predated by P. However, in the dynamics of N_2 we find that the actual overlap coefficient is $(b - \epsilon)$ rather than b. Hence the parameter ϵ measures the degree to which N_2 can more successfully avoid predation in comparison to N_1. Since this system seeks to model the dynamics of two prey species and their common predator, we impose an upper bound on ϵ, such that the term $(b - \epsilon)$ is positive. If this condition were not satisfied, we would find that N_2 predates upon P, which is a system of entirely different character.

The parameters c and d occur only in the differential equation for P and gives the growth and death rates for the predator, respectively.

For the numerical simulations in this project, the system parameters will be:

- $\alpha = 1.5$
- $b = 0.01$
- $c = 0.5$
- $d = 1.0$
- $r = 1.0$
- $\epsilon = 0.009$

unless otherwise noted. And except for special cases, most simulations will be initiated at the point $(N_1, N_2, P) = (580, 580, 50)$.

2 Dynamics in the absence of the predator

We consider the cases $\alpha > 1$ and $\alpha = 1$ separately.

2.1 The funnel trap ($\alpha > 1$)

By initializing the system at $P_0 = 0$ we obtain the reduced system:

$$\dot{N_1} = N_1 \cdot (r - \frac{r}{k}N_1 - \frac{r}{k}N_2) \tag{5}$$

$$\dot{N_2} = N_2 \cdot (r - \frac{r}{k}\alpha N_1 - \frac{r}{k}N_2) \tag{6}$$

We can visualize this system and its nullclines on the plane:

$$N_1 = 0 \tag{7}$$

$$\frac{r}{k}N_1 + \frac{r}{k}N_2 = r \tag{8}$$

$$N_2 = 0 \tag{9}$$

$$\frac{r}{k}\alpha N_1 + \frac{r}{k}N_2 = r \tag{10}$$

where (7),(8) and (9),(10) are the nullclines for N_1 and N_2 respectively. They are color coded in Figure 1.

As can be seen, there are only three fixed point solutions which correspond to:

- $(N_1, N_2)^* = (0, 0)$: Mutual extinction.
- $(N_1, N_2)^* = (k, 0)$: N_1 drives N_2 into extinction.
- $(N_1, N_2)^* = (0, k)$: N_2 drives N_1 into extinction.

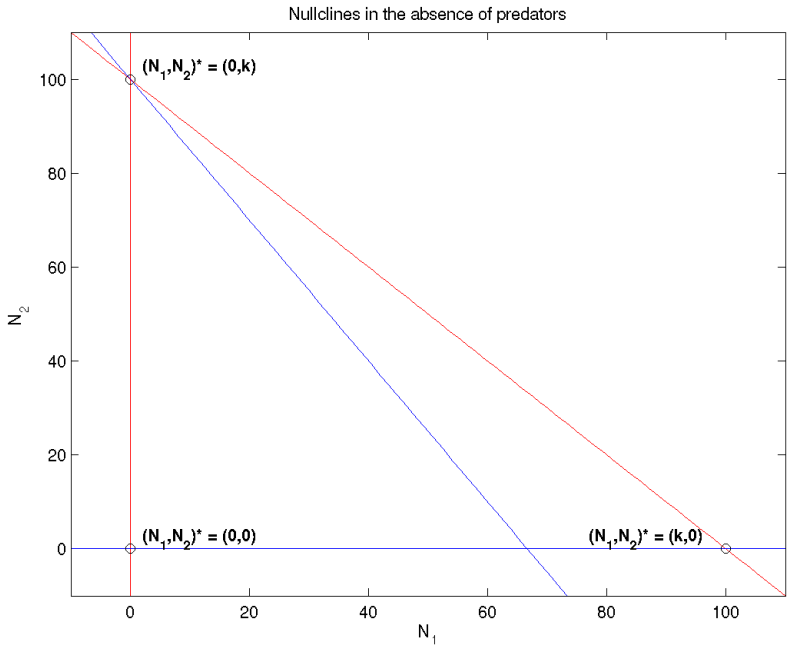

Figure 1: The nullclines of the N_1, N_2 system in the absence of predators. Red: $\dot{N}_1 = 0$; Blue: $\dot{N}_2 = 0$

This result immediately shows that in the reduced N_1, N_2 system there is *no* fixed point that allows for mutual coexistence for N_1 and N_2. Thus, for this model, we have verified Gause's comment that when a single species posesses a sole advantage over its competitor, there cannot be a steady state solution involving *both* N_1 and N_2.

As the $\alpha > 1$ condition enhances N_1 with respect to N_2, we may expect that the only *stable* solution among the three is $(N_1, N_2)^* = (k, 0)$. Linear analysis verifies this suggestion, revealing the Jacobian matrices:

$$J^*(k,0) = \begin{pmatrix} -r & -r \\ 0 & -r(\alpha - 1) \end{pmatrix} \tag{11}$$

$$J^*(0,k) = \begin{pmatrix} 0 & 0 \\ -r & -r \end{pmatrix} \tag{12}$$

for $(k, 0)$ and $(0, k)$ respectively. Unfortunately, the zero entries leave the analysis slightly ambiguous. For instance, the linearization tells us little about the result of a small displacement on $\delta\dot{N}_1$, i.e. the horizontal stability of $(0, k)$. We are luckier at the origin, however, where the linearized stability turns out to be:

$$\begin{pmatrix} \delta\dot{N}_1 \\ \delta\dot{N}_2 \end{pmatrix} = \begin{pmatrix} r & 0 \\ 0 & r \end{pmatrix} \cdot \begin{pmatrix} \delta N_1 \\ \delta N_2 \end{pmatrix} \tag{13}$$

which shows that near the origin the components of the displacement vector δN_1 and δN_2 are decoupled and are unstable in both, in the so-called "star" geometry.

For a more conclusive statement regarding the stability of the remaining fixed points, we consider the phase plane instead from a geometric perspective. Taking into account the signs of $\dot{N}_1$ and $\dot{N}_2$ in each region of the plane defined by the nullclines gives Figure 2.

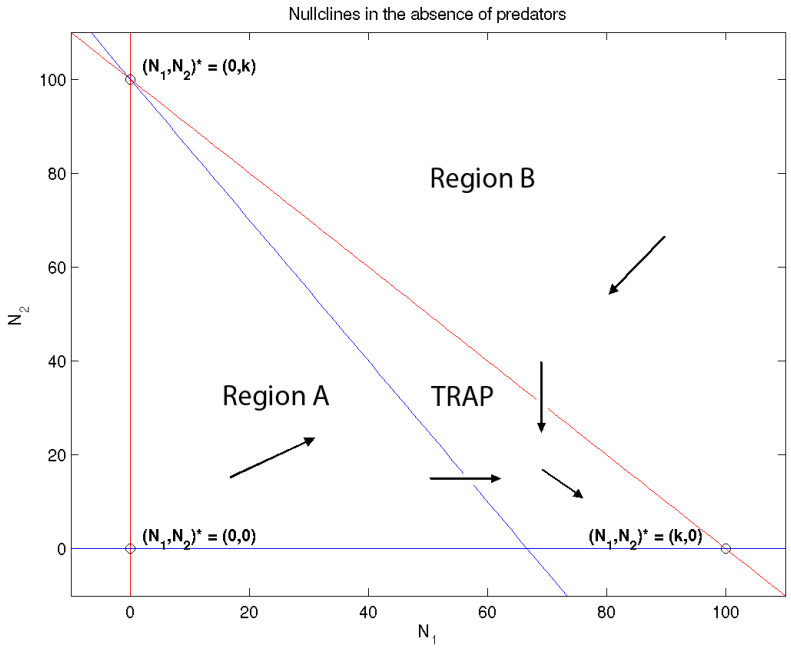

Figure 2: Representative vectors indicating the flow are plotted for each region defined by the nullclines.

In each region and along each nullcline, we expect the direction of the flow to be as described by the representative vectors above. We can immediately interpret the space between the two sloped nullclines as a funnel that traps all trajectories that begin in the first quadrant and leads them to the fixed point at $(k, 0)$. To see this, consider a trajectory that begins in the region marked A. The trajectory is continuously pushed to the right until it enters the trap and finds itself unable to cross the nullcline $N_2 = k - N_1$. And, since everywhere in the trapping region $\dot{N}_1$ is positive and $\dot{N}_2$ is negative, this trajectory *must* approach the fixed point at $(N_1, N_2)^* = (k, 0)$ asymptotically.

Likewise, a trajectory that begins in region B is initially attracted to the trapping region but finds itself unable to escape past the nullcline $N_2 = k - \alpha N_1$; and in time it likewise dwindles to $(N_1, N_2)^* = (k, 0)$. Typical cases of these two trajectories are shown in Figure 3.

The above argument shows that for the N_1, N_2 system in the absence of predators, there is absolutely *no* possible coexistence between N_1 and N_2. Firstly, we find that variations in r have no effect in the qualitative geometric features of the N_1, N_2 phase space. (Obviously, b, ϵ, c, d are also meaningless when $P = 0$.) Furthermore, variations in k and $\alpha > 1$ within their parameter ranges only stretch and shrink the funnel *without* changing its general behavior. In this way N_1 is quite the unpleasant neighbor, stubbornly unwilling to share living space under any conditions.

In conclusion, in the absence of the predator, the only possible long term solution is $(N_1, N_2)^* = (k, 0)$, i.e. complete domination by N_1, *regardless* of the system parameters, including system size k.

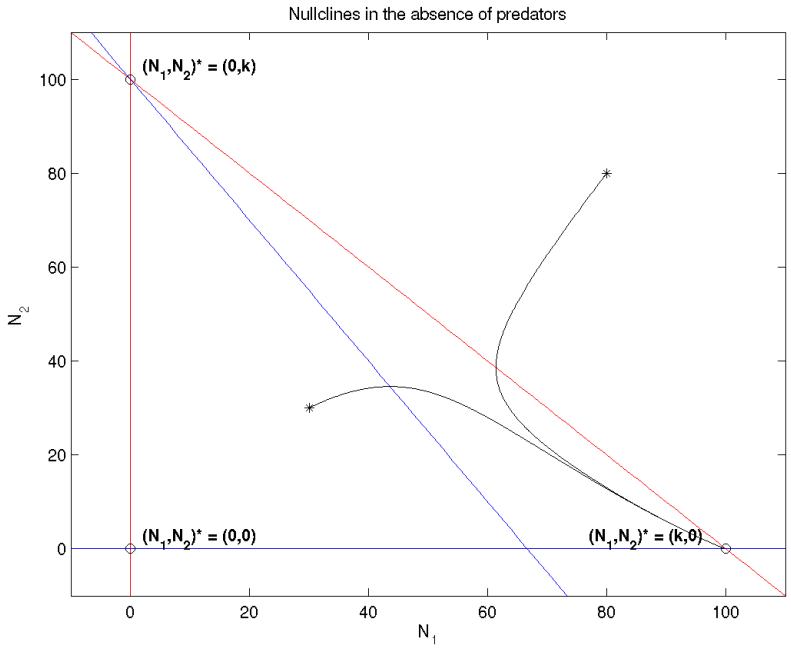

Figure 3: Typical trajectories in the N_1, N_2 plane. The trapping effect is clearly observed.

2.2 Symmetric case ($\alpha = 1$)

For completeness, we consider now the (rather uninteresting) case when $\alpha = 1$, for which the governing equations become symmetric:

$$\dot{N_1} = N_1 \cdot (r - \frac{r}{k}N_1 - \frac{r}{k}N_2) \tag{14}$$

$$\dot{N_2} = N_2 \cdot (r - \frac{r}{k}N_1 - \frac{r}{k}N_2) \tag{15}$$

This scenario corresponds to the case where the curves defining the funnel trap have coalesced and the trap is nonexistent.

By considering the sum $N_s = N_1 + N_2$, we obtain from the above system a decoupled logistic equation in N_s, which can be easily solved analytically. Using this result, then, gives a separable equation in $\dot{N_s}$ where $N_s = N_1 - N_2$. Hence, the symmetric case is amenable to a full analytic solution for all t. However, the ultimate behavior of this special case is rather apparent without much work: trajectories that begin in the first quadrant will land somewhere along the superposition of the two nullclines at $N_1 + N_2 = k$. Clearly, linear analysis at any of such solutions will give a "comb" stability.

For the remainder of the paper, I will generally assume that $\alpha > 1$.

2.3 Introduction of the predator: The trap fails!

Postponing the theoretical development until the following section, we can visualize the dynamics of the full (N_1, N_2, P) system simply through projections onto the N_1, N_2 plane. For the diagram below, I have fixed k, i.e. the capacity of the system, at 300 units. The initial state of the system is: $(N_1, N_2, P)_0 = (80, 80, p)$ where $p = P_0$ is the parameter being varied.

As stated previously, in the absence of the predator, N_1 posesses a competitive advantage over N_2 and as expected completely conquers the environment. However, $\epsilon > 0$ in the presence of the predator represents a *different* scenario in which N_2 has its own particular superiority over N_1. We can now expect the resulting interplay to be much richer, as the new dynamics represents a more 'fair' competition between N_1 and N_2. Since N_2's advantage depends on the instantaneous predator population, the $\epsilon > 0$ advantage is generally not as simple to visualize as $\alpha > 1$ which takes the form of a static, trapping region in the N_1, N_2 plane. Since N_2's advantage is in more successfully avoiding the predator, its competitive edge should be enhanced as the predator population increases. And, obviously, in the absence of the predator N_2 is entirely at the mercy of N_1.

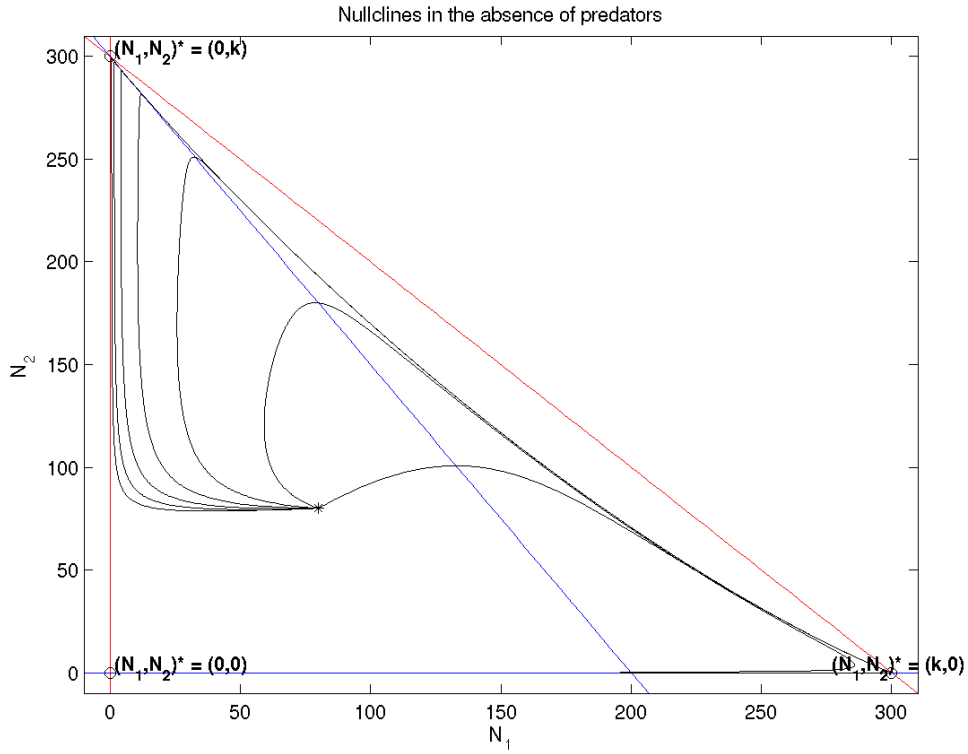

Figure 4: With increasing predator populations, the trap becomes less significant and trajectories may escape the trapping region. In fact, some even converge, within numerical error, to the fixed point (top left) representing N_2's triumph and N_1's demise.

In Figure 4, the evolution of $(N_1, N_2, P) = (80, 80, p)$ is shown on the plane. p is increased in increments of 100. As before, $p = 0$ results in a trajectory that collapse neatly into the trap. Higher values of p lead the trajectories towards the fixed point on the N_2 axis.

We have now discussed at some length the two advantages that N_1 and N_2 posess over one another. Since

the full N_1, N_2, P system represents a more 'fair' struggle between N_1 and N_2, it seems plausible if not obvious that we will enounter richer dynamics, including possibly a stable coexistence between the three species, contrary to Gause's principle.

In other words, perhaps in the full system it may be possible for a 'big town' to support both you and me.

3 Full N_1, N_2, P dynamics

Analysis of the three-dimensional system turns out to be algebraically cumbersome. Still, the standard techniques of systems analysis can be applied rather procedurally.

3.1 Nullcline analysis

By inspection, the dynamical system,

$$\dot{N_1} = N_1 \cdot (r - \frac{r}{k}N_1 - \frac{r}{k}N_2 - bP) \tag{16}$$

$$\dot{N_2} = N_2 \cdot (r - \frac{r}{k}\alpha N_1 - \frac{r}{k}N_2 - (b-\epsilon)P) \tag{17}$$

$$\dot{P} = P \cdot (cbN_1 + c(b-\epsilon)N_2 - d) \tag{18}$$

yields the following nullplanes:

$$N_1 = 0 \tag{19}$$

$$\frac{r}{k}N_1 + \frac{r}{k}N_2 + bP = r \tag{20}$$

$$N_2 = 0 \tag{21}$$

$$\frac{r}{k}\alpha N_1 + \frac{r}{k}N_2 + (b-\epsilon)P = r \tag{22}$$

$$P = 0 \tag{23}$$

$$cbN_1 + c(b-\epsilon)N_2 = d \tag{24}$$

If we select a 3-tuple of nullplanes, each arising from each of equations (16), (17) and (18), we obtain a system of equations that can be solved for the fixed points of the full system. As it turns out, there are only 6 unique solutions resulting from such combinations. The first three are of little interest to us now, as we've encountered them already in the previous section while studying the evolution of N_1 and N_2 in the absence of P. They are (again):

- $(N_1, N_2, P)^* = (0, 0, 0)$: Mass extinction.
- $(N_1, N_2, P)^* = (k, 0, 0)$: N_1 drives N_2 into extinction.
- $(N_1, N_2, P)^* = (0, k, 0)$: N_2 drives N_1 into extinction.

The following two are only slightly more interesting. They represent the interaction of *one* of the prey species with the predator:

- $(N_1, N_2, P)^* = (\frac{d}{bc}, 0, \frac{r}{b}(1 - \frac{d}{kcc})$: Only N_1 and P left.
- $(N_1, N_2, P)^* = (0, \frac{d}{(b-\epsilon)c}, \frac{r}{b-\epsilon}(1 - \frac{d}{kc(b-\epsilon)})$: Only N_2 and P left.

Finally, the fixed point solution that will occupy the remainder of this paper is the one arising from the three nontrivial nullplanes of the system, i.e. the fixed point that solves the following equation:

$$\begin{pmatrix} \frac{r}{k} & \frac{r}{k} & b \\ \frac{r}{k}\alpha & \frac{r}{k} & (b-\epsilon) \\ cb & c(b-\epsilon) & 0 \end{pmatrix} \cdot \begin{pmatrix} N_1 \\ N_2 \\ P \end{pmatrix} = \begin{pmatrix} r \\ r \\ d \end{pmatrix} \tag{25}$$

For example, for the standard set of parameters and $k = 400$, this fixed point turns out to be $(N_1, N_2, P)^* \approx (189.47, 105.26, 26.31)$ and appears to be stable in numerical simulations. The reason for our particular interest in this solution is because this fixed point represents the coexistence solution that was outlawed in the (N_1, N_2) case by Gause's principle. In the full dynamics of (N_1, N_2, P) we find that there *is* in fact a possible coexistence between the prey. As remarked earlier, this development is not so surprising (especially considering the specific wording of Gause's principle – "coexistence is possible if environment exploited *differently*") since α represents N_1's advantage, while ϵ favors N_2.

Further justification for our special attention to this fixed point comes from the fact that the more complicated attractors that one finds for higher values of k develop from the instabilities at this location. This proposition will be quantified in the upcoming sections.

3.2 How big is big enough?

We now answer the question that opened this assigment. Given that there is now the possibility of mutual coexistence, does the size of the 'town' (i.e. k) determine whether two species can coexist?

We must first establish the range of k for which the fixed point under consideration actually gives a sensible solution to our problem. In the context of populations, this simply requires all three quantities N_1^*, N_2^*, P^* be nonnegative. While a symbolic treatment of the solution turns out to be much too cumbersome, the fixed point is in principle parametrized by k and is given by the equation (merely a rewritten form of Eq. 25):

$$\begin{pmatrix} N_1 \\ N_2 \\ P \end{pmatrix} = \begin{pmatrix} \frac{r}{k} & \frac{r}{k} & b \\ \frac{r}{k}\alpha & \frac{r}{k} & (b-\epsilon) \\ cb & c(b-\epsilon) & 0 \end{pmatrix}^{-1} \cdot \begin{pmatrix} r \\ r \\ d \end{pmatrix} \tag{26}$$

We then evaluate the curve traced by Eq. 26 in Figure 5.

Evidently, for small values of k, N_2^* is negative and this fixed point does *not* give a realistic solution to our population problem. Plotting N_2 against k reveals a surprisingly simple relationship between N_2^* and k (Figure 6). Solving this linear relationship in our particular parameter set reveals that $k_{crit} \approx 311.5$. Apparently, the town must be approximately 312 'units' large for the both of us!

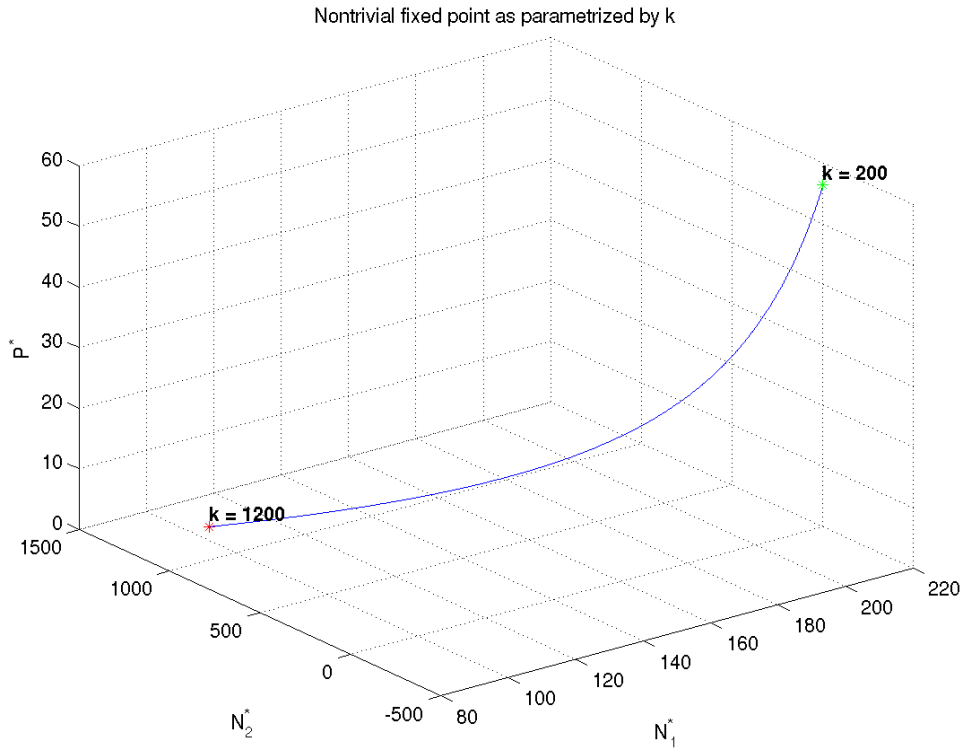

Figure 5: Nontrivial fixed point as a parametrized curve for $200 \leq k \leq 1200$

3.2.1 General case

Motivated by the apparent linearity of $N_2^* = f(k)$ in Figure 6, I have considered $N_2^* = f(k)$ symbolically. This yields:

$$N_2^* = f(k) = \frac{\epsilon b}{\epsilon^2 - b(\alpha - 1)(b - \epsilon)} k - \frac{b(\alpha - 1) + \epsilon}{dc\,[\epsilon^2 - b(\alpha - 1)(b - \epsilon)]} \tag{27}$$

For now, let us take the existence of a nonnegative N_2 as the sole criterion for the existence of a valid nontrival fixed point. (Note that we have yet to discuss stability at all!) We'll also assume that our parameter set is such that the intercept of f is negative, i.e. that the constant term in Eq. 27 is negative. Since the numerator (and d and c) are always positive given our parameter ranges, this requires:

$$M = \epsilon^2 - b(\alpha - 1)(b - \epsilon) > 0 \tag{28}$$

However, the condition in Eq. 28 is not generally true. For the standard parameter values set forth in Section 1, $M = 7.6 \times 10^{-5} > 0$ and hence N_2 becomes nonnegative for some $k > k_{crit}$. On the other hand, suppose instead that $\epsilon = 0.001$. In that case, we obtain $M = -4.4 \times 10^{-5} < 0$. This possibility, along with Eq. 27, suggests that for a different set of parameters we may find coexistence for *smaller* values of $k < k_{crit}$, as N_2 begins nonnegative for small k and becomes negative for larger k. While this possibility is interesting, it will

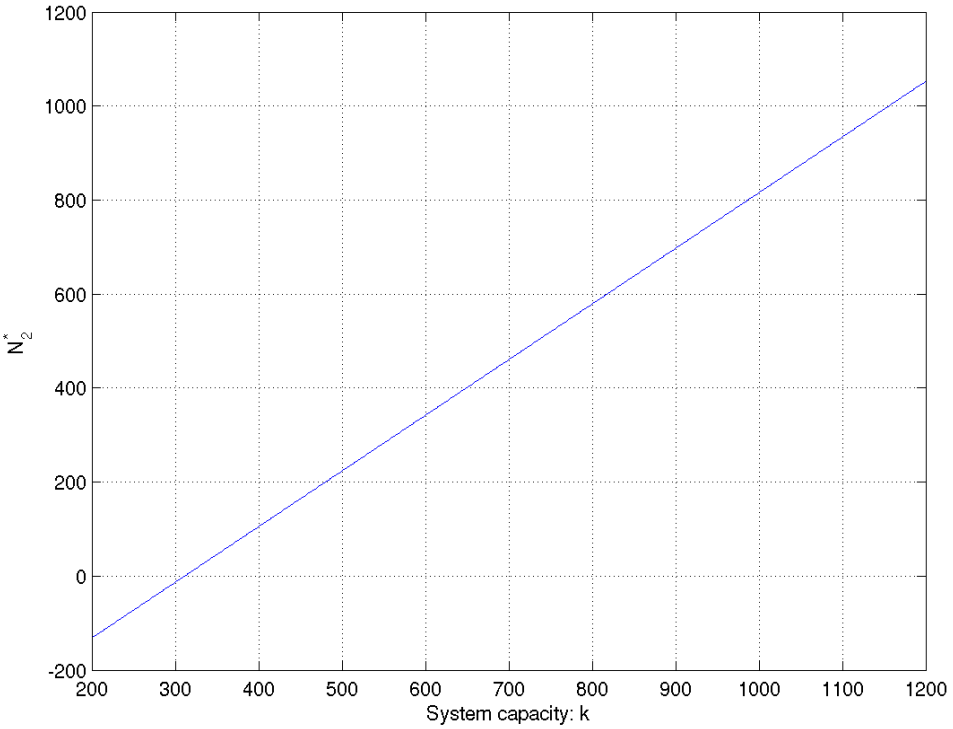

Figure 6: The parametrization of N_2^* by k is linear.

not be considered further. Instead, we will simply assume that in our systems, $N_2 > 0$ only for $k > k_{crit}$ (or, equivalently, that the inequality in Eq. 28 holds).

We then solve for k_{crit}:

$$k_{crit} = \frac{ab - (b - \epsilon)}{bcd\epsilon} \tag{29}$$

This expression gives the critical value of k above which the system produces a valid, nontrivial fixed point. Unfortunately, Eq. 29 is not so useful due to the arbitrary assumptions that we have made in the analysis. However, the finding of the parameters c and d in the expression for k_{crit} is unexpected and interesting, indicating a lower k_{crit} as the parameters controling the flow of the predator population is increased.

3.3 Stability

In the previous sections, attention was paid to the movement of the nontrivial fixed point into the first quadrant of phase space. We now ask about its linear stability. To answer this question, consider again the system:

$$\dot{N}_1 = rN_1 - \frac{r}{k}N_1^2 - \frac{r}{k}N_1N_2 - bN_1P \tag{30}$$

$$\dot{N}_2 = rN_2 - \frac{r}{k}\alpha N_1N_2 - \frac{r}{k}N_2^2 - (b-\epsilon)N_2P \tag{31}$$

$$\dot{P} = cbN_1P + c(b-\epsilon)N_2P - dP \tag{32}$$

and its Jacobian matrix:

$$J^* = \begin{pmatrix} r - 2\frac{r}{k}N_1^* - \frac{r}{k}N_2^* - bP^* & \frac{-r}{k}N_1^* & -bN_1^* \\ \frac{-r}{k}\alpha N_2^* & r - 2\frac{r}{k}N_2^* - \frac{r}{k}\alpha N_1^* - (b-\epsilon)P^* & -(b-\epsilon)N_2^* \\ cbP^* & c(b-\epsilon)P^* & cbN_1^* + c(b-\epsilon)N_2^* - d \end{pmatrix} \tag{33}$$

However, as $(N_1, N_2, P)^*$ solves Eq. 25, we can simplify the above with:

- $\frac{r}{k}N_1^* + \frac{r}{k}N_2^* + bP^* = r$
- $\frac{r}{k}\alpha N_1^* + \frac{r}{k}N_2^* + (b-\epsilon)P^* = r$
- $cbN_1^* + c(b-\epsilon)N_2^* = d$

and obtain:

$$J^* = \begin{pmatrix} -\frac{r}{k}N_1^* & \frac{-r}{k}N_1^* & -bN_1^* \\ \frac{-r}{k}\alpha N_2^* & -\frac{r}{k}N_2^* & -(b-\epsilon)N_2^* \\ cbP^* & c(b-\epsilon)P^* & 0 \end{pmatrix} \tag{34}$$

As usual, the characteristic equation is given by

$$det(J^* - \lambda I_3) = 0 \tag{35}$$

Since all of the entries in J^* are either constants or are parameterized through k, in principle Eq. 35 represents the roots of a cubic-function in λ whose coefficients are parametrized by k. Again, a symbolic treatment is far too laborious, so we resort to a numerical approach as described in the following section.

3.3.1 Approach

As always, the quantities of interest are the real parts of the eigenvalues, which are determined by Eq. 35. We will tease them out as follows:

1. Consider $det(J^* - \lambda I_3) = f(\lambda)$ over the real line. Since the coefficients of the cubic polynomial are all real, we must have at least one real root. Obtain this root, λ_R, by interpolation.

2. Numerically factor out the term $(\lambda - \lambda_R)$ from the cubic. From the resulting quadratic, deduce the real parts of the complex roots by calculating the vertex of the parabola.

   (Remark: Let $\lambda_{C^\pm}$ represent the complex roots. By the quadratic formula, we have $Re\left[\lambda_C\right] = Re\left[\lambda_{C^\pm}\right] = -\frac{b}{2a}$ where a and b are the coefficients associated with the quadratic and linear terms, respectively. From basic calculus, we have that the vertex of a parabola is given by $-\frac{b}{2a}$. Hence:

$$Re\left[\lambda_C\right] = \lambda_V \tag{36}$$

   where λ_V is the vertex of the quadratic.)

A typical plot resulting from the above procedure is pictured in Figure 7. The computational details and the scripts used in the calculation are reported in Appendix 1 of this assignment. Here, we merely state some of the results:

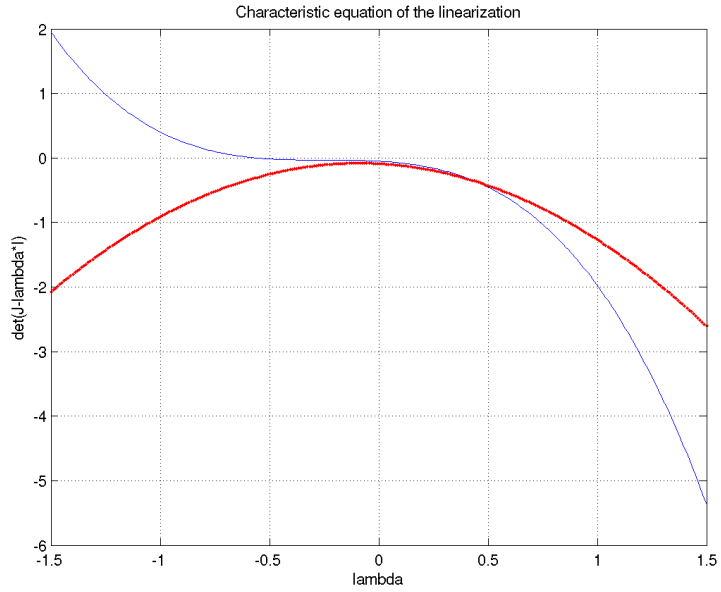

Figure 7: The cubic function $det(J^* - \lambda I_3) = f(\lambda)$ (solid blue). The red dots traces the quadratic equation that results from: $\frac{f(\lambda)}{\lambda - \lambda_R}$. $Re(\lambda_C)$ is obtained by considering the vertex of this quadratic.

k	λ_R	$Re(\lambda_C)$
300	0.03051893166903	-0.32887555750354
310	0.00319373625057	-0.32228363414204
311.1	0.00001201063378	-0.32168591081887
311.11111...	-0.00002013337241	-0.32178722300964
312	-0.00250920098777	-0.32028260248924
350	-0.16946825476467	-0.26019842172357
375	-0.42103166966124	-0.14692910730032
400	-0.55943779280922	-0.08869650680063
425	-0.64098233317196	-0.05759456829995
450	-0.69811479991791	-0.03763337625298
475	-0.74126341079928	-0.02374935563374
500	-0.77530885078003	-0.01365102428031
525	-0.80293799603971	-0.00610204281474
550	-0.82584020472873	-0.00035595010773
551	-0.82666937586320	-0.00015662851995
551.79463	-0.82732067328578	-0.00000000095928
552	-0.82748872440641	0.00004029256492
553	-0.82830539969215	0.00023540570821
554	-0.82911941270112	0.00042873020269
555	-0.82993077435794	0.00062028508698
560	-0.83391442890901	0.00154948535598
575	-0.84507461106758	0.00406453131344

From the previous section, we have $k_{crit} = \frac{2800}{9} \approx 311.11111....$ Evaluation of λ_R and $Re(\lambda_C)$ at k_{crit} gives negative values, which indicates that our fixed point is stable *as soon* as it appears in the first quadrant. As we continue to increase k, we find that λ_R remains negative, while $Re(\lambda_C)$ becomes positive at $k^* \approx 551.79463$.

For our parameter set, we have a linearly stable fixed point representing coexistence of N_1 *and* N_2 as long as the capacity of the system remains in the interval: $311.11111... < k < 551.79463$

4 More complicated dynamics

4.1 Limit cycle

As $k \to k^*$ the rate of approach to the fixed point slows. As the capacity of the system is increased even further, we develop a small limit cycle about the fixed point. These two effects can be observed in the time series in N_1 for parameter values of 540, 550, and 560 (Figure 8).

And in Figure 9 , we see the development of the limit cycle in phase space.

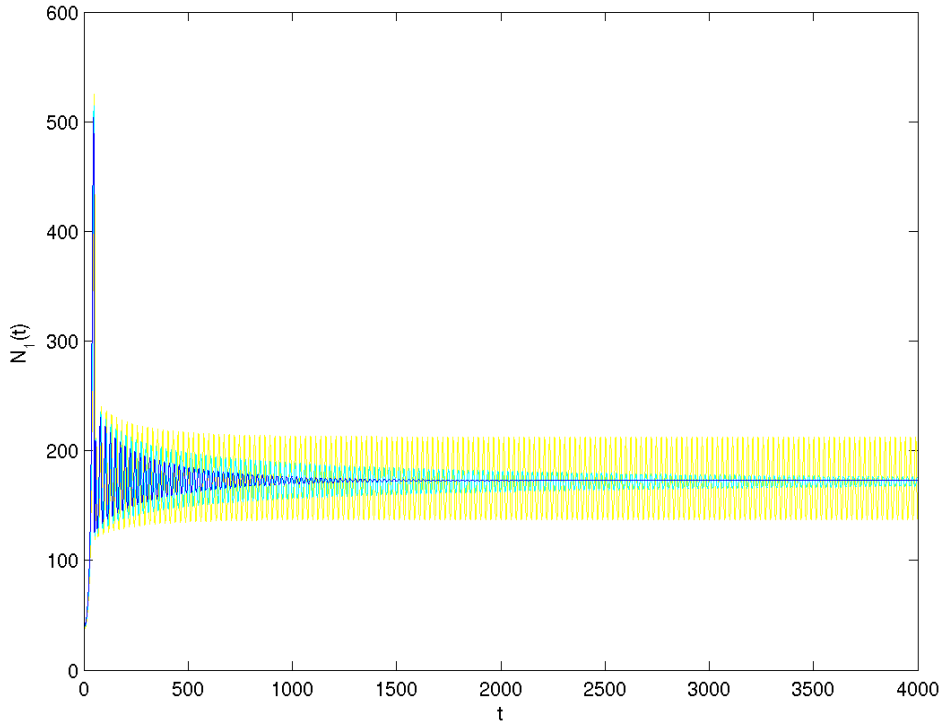

Figure 8: The time evolution of $N_1(t)$ for three separate parameter sets $k = 540$ (blue), $k = 550$ (cyan) and $k = 560$ (yellow). Note the emergence of the limit cycle. Each calculation shares the common starting condition of $(N_1, N_2, P)_0 = (580, 580, 50)$

4.2 Period doubling

Instabilities of the fixed point at $k = k^*$ result in the development of a limit cycle. The central question now is to ask how does the cycle's qualitative properties react to further increases in k. Given the growing instability ($Re(\lambda_C)$ becomes more positive) of the fixed point for higher k, it is reasonable to expect that the size of the circuit will expand. However, another familiar response to variations in parameter is the period doubling in which the trajectory completes 'additional turns' before closing on itself. This effect is best characterized by a Poincaré section of the attractor.

Indeed, if we take a Poincaré plane through the fixed point, the development of the limit cycle could in fact be considered the *first* period doubling at $k = k_1^* \approx 552$. As k moves past k_1^*, the section would reveal the solitary point (representing the fixed point) splitting into two (since the cycle must pass the plane at two distinct locations). For the Poincaré sections that follow, I have taken the slice plane to be $N_1 = N_1^*$.

Admittedly, my initial search was pure blind, numerical 'exploration.' Luckily, I managed to find the second period doubling at about $k = k_2^* \approx 796$. In this context, a period doubling occurs when a single point in the Poincaré section diverges into two new points, as seen in Figure 10.

Additional numerical explorations reveal the third and fourth period doubling points to be approximately:

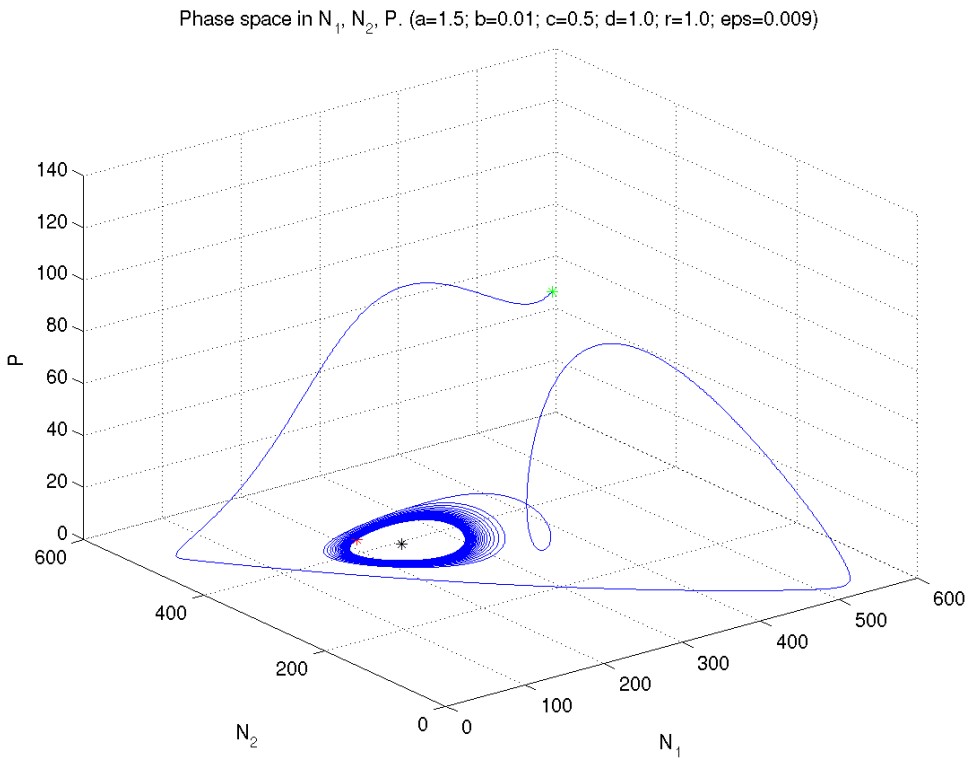

Figure 9: Limit cycle about the fixed point (black asterisk) for $k = 560$. The initial condition is marked in green; the terminating position ($t = 4000$) is marked in red.

k_1^*	552
k_2^*	796
k_3^*	850
k_4^*	862

The additional critical points are calculated in exactly the same manner; that is, by inspection of the Poincaré sections. The data in the form of the Poincaré sections are supplied in Appendix 2.

While we posess only a very limited and very approximate set of the doubling points, we note that the spacing between successive points appear to descrease geometrically with a common factor, $\delta_{experimental}$, that is highly reminiscent of Feigenbaum's constant.

- $\Delta k_2 = k_2^* - k_1^* = 244$
- $\Delta k_3 = k_3^* - k_2^* = 54$
- $\Delta k_4 = k_4^* - k_3^* = 12$

$$\delta_{experimental} \approx \frac{\Delta k_2}{\Delta k_3} \approx \frac{\Delta k_3}{\Delta k_4} \approx 4.5 \tag{37}$$

The evidence considered above is hardly conclusive. However, I will make the leap of faith that the mechanism of period doubling for this system posesses a unimodal, quadratic maximum return map. Taking this for granted and using the real Feigenbaum's constant, δ_F, we now compute the accumulation point for the doubling.

Since $\Delta k_i = k_i^* - k_{i-1}^*$, we have:

$$\begin{aligned} k_\infty^* &= k_3^* + \Delta k_4 + \Delta k_5 + \Delta k_6 + ... \\ &= 850 + 12 + 12\frac{1}{\delta_F} + 12\frac{1}{\delta_F^2} + ... \\ &= 862 + 12\sum_{i=0}^{\infty} \frac{1}{\delta_F}^i \\ &\approx 865.3 \end{aligned}$$

The accumulation point k_∞^* calculated above must be taken as a *very* approximate value. First of all, $\delta_{experimental} < \delta_F$, which implies that we *overestimate* the geometric contraction of the critical values (and hence underestimate k_∞^*). But the even bigger problem lies in the validity of the first four k_i^* themselves: I certainly would not bet my life on them.

Nevertheless,

> For large enough system capacity $k > k_\infty^* \approx 865$ there is possibility for a *chaotic* attractor in the N_1, N_2, P system. The chaotic attractor likely develops through period doubling that originates from the instabilities of the fixed point defined by Eq. 25.

4.3 Chaos

We consider the case $k = 925$, which is well beyond k_∞^* as calculated in the previous section. Starting from the initial condition of $(N_1, N_2, N_3)_0 = (580, 580, 50)$ reveals a flow of remarkable complexity in comparison to the previous trajectories (Figure 11).

As expected, consideration of the resulting time series (after allowing the transients to decay, of course) shows a very complicated signal (Figure 12) with a frequency spectrum that lacks particularly dominant frequencies, i.e. aperiodicity. The power spectrum for N_1, N_2, P are provided in Appendix 3.

For the remainder of this section we will consider the quantitative properties of this attractor. Before doing so, however, I will remark on a few oddities of the chaotic attractor in terms of the population context.

- While the details of the dynamics are obviously very complicated, the evolution of $N_1(t) + N_2(t)$ with $P(t)$ appears to follow typical predator-prey models, i.e. the population of the prey accumulates in the absence of the predator; after reaching some critical mass, the predator population becomes explosive, leading to prey decimation and ultimately the predator's own demise; the pattern repeats.
- The sum of prey populations, $N_1 + N_2$ hovers around $k \approx 925$, the system capacity.
- A statistical description of $P(t)$ generally clumps around very low values of P. In other words, the quantity of predator present at any moment is likely to appear miniscule in comparison to that of the prey populations. These two claims are quantified in the histogram (Figure 13).

- Statistical distribution of the individual prey populations (Figure 14) shows that N_2 typically dominates over N_1 in the chaotic attractor!

4.3.1 Lyapunov exponent

We now ask the attractor whether it is truly "chaotic." By this, we check whether the attractor possesses the crucial property of sensitivity to initial conditions. As usual, this is achieved by computation of the Lyapunov exponent of two nearby trajectories.

To make certain that the two initial conditions are points *on* the attractor, I have used the point resulting from a typical run ($t_{span} = 4000$):

- $(N_1, N_2, P) = (68.474958970987, 808.625354491878, 5.298503037936)$
- $(N_1 + \delta, N_2, P) = (68.474958970987 + 1 \times 10^{-12}, 808.625354491878, 5.298503037936)$

As seen in Figure 15, the exponent turns out to be roughly: $\lambda_L = 4.724 \times 10^{-3} > 0$, indicating exponential divergence of nearby trajectories and that the system is indeed chaotic at $k = 925$.

4.3.2 Attractor dimension

In this assignment, the governing equations of the system were given as the starting point. Hence, it would not only be feasible, but also very natural, to compute the attractor dimension by a correlation dimension algorithm in N_1, N_2, P space. However, since a program already exists for the dimensional calculation from a single time series (courtesy Prof. Rothman and 18.353 staff), we will use the latter technique.

This routine calculation reveals the attractor dimension to be roughly: $D = 1.023$.

This particular number is plausible, although it is likely too low. This chaotic attractor is an object that lives in the three dimensional space of N_1, N_2 and P, but, as seen by the Poincaré sections, certainly does not appear to make up a two-dimensional manifold. Hence, we expect some fractional dimension in the range $1 < D < 2$.

4.4 Even larger k

The finding that the population composition of the prey species shifts in favor of N_2 (Section 4.3) motivates this line of thought.

As it turns out, this curious phenomenon may have been forecast (although it is by no means obvious) by Eq. 27 which shows that, under the assumptions that we have made regarding M (Eq. 28), N_2^* *increases* linearly with respect to k. In other words, the nontrivial fixed point shifts to favor N_2 over N_1 as the carrying capacity is enlarged. In fact, the projection of $(N_1, N_2, P)^* = \vec{f}(k)$ on the (N_1, N_2) plane shows a linear trace towards larger N_2. (Figure 16).

Interestingly, we also find that our requirement that the fixed point remain in the first quadrant imposes an additional condition of $k < k'_{crit} \approx 2000$. For higher values of k, trajectories generally seem to converge

to the fixed point involving only N_2 and P. (This fixed point was briefly mentioned in Section 3.1.) So, surprisingly, we find that it *is* possible for the town to be *too* big for the both of us! Therefore, this sole counterexample leads us to conclude that the familiar saying – which, coincidentally, is also the title of this project – is misleading and incomplete!

As the length of this document is becoming obscenely long, we will consider 'large' k to be those in the range $k > 1500$, but we will not venture beyond $k'_{crit} \approx 2000$.

Remarkably, the phenomenon of N_2's dominance in large k is also explained by the very fixed point that we have considered throughout this assignment. This is so, because for large k, the stability of the fixed point tends to be *restored*! Numerical computation of the eigenvalues for large k reveals a shape as in Figure 17. The plot clearly indicates the return of $Re(\lambda_C)$ into the negative region in the vicinity of $k \approx 2000$. As it happens, at $k = 2000$, we have $Re(\lambda_C) = -4.099 \times 10^{-6}$, revealing that the fixed point likely becomes stable just before it leaves the first quadrant.

Numerical simulations actually reveal that $Re(\lambda_C) < 0$ isn't a *necessary* condition for fixed point-like behavior. For $k = 1980$, for example, we have $\lambda_R \approx -0.9998$ and $Re(\lambda_C) \approx 2.609 \times 10^{-4} > 0$. Still, initiating the system at (580,580,50) produces a flow that appears to converge to the fixed point, despite its linear instability. A closer examination shows that the trajectory actually undergoes erratic oscillations in the *very* close vicinity of the fixed point. However, in the macroscopic view as in Figure 18, the flow virtually behaves like an attracting fixed point.

In this section, we have made the entirely unexpected discovery that for large k i.e. habitats of large capacity, N_2 actually dominates over N_1!

5 Near absence of the predator

We now discuss some of the absolutely *bizarre* consequences that arise from some of the findings so far.

- The nontrivial fixed point enters the first quadrant of phase space at $k = k_{crit}$ and exits at $k = k'_{crit}$ near the N_2 axis. As k approaches k'_{crit}, the 'general stability' of the fixed point is restored, which indicates that for appropriate values of k, there is a steady state solution that favors N_2 over N_1.
- As can be seen in the parametrization of the fixed point in Figure 5 and the histograms in Figure 13, the steady-state level of P^* is generally very low in comparison to the size of prey populations. As a matter of fact, the 'fixed point' at $k = 1980$ yields: $(N_1, N_2, P)^* \approx (68, 809, 5.3)$. Intuitively speaking, then, it appears that the predator *cannot* be exerting an incredible amount of pressure on the prey populations.
- In the *complete* absence of the predator, the sole determinant of competitive success is the parameter $\alpha > 1$ that enables domination by N_1. We have seen that no other parameter can change this outcome. This was observed in the static 'trap' that attracts trajectories on the N_1, N_2 plane towards $(k, 0)$.

Combining the above considerations then yields:

For certain capacities, we may have a steady solution favoring N_2 over N_1 in the *near* absence of the predator. For me, this is entirely unexpected as the competitive advantage of N_2 should diminish in the limit of small P. Furthermore, we have considered the case of *complete* absence which revealed, quite naturally, that *only* N_1 can survive in the long run. On the other hand, if certain parameter choices (i.e. large k) allow N_2 to

dominate N_1 *even* in the limit of arbitrarily low P, then the qualitative features of phase space seems to be *discontinuous* in the vicinity of the plane $P = 0$.

Given the precariousness of this phase space, then, there are further questions:

(In the systems we have considered over this term, I have always been interested in the effects of changing a system parameter mid-simulation. In principle, these types of manipulations are not fundamentally novel since one can think of this as simply two separate simulations connected by a mutual final and initial points. Yet, interpreting the system response of such a parameter change in the context of the model often yields interesting [or, at the very least, slightly amusing] scenarios.)

The ideas developed in this project seems to indicate the possibility of certain species that are successful in their habitat solely due to a fortunate accident in some effective parameter of their environment, such as its size. (This occurs for N_2 when $k \approx k'_{crit}$.) This implies that, for instance, the response by a system of species suffering endangerment through human encroachment may not be merely a reduction in the scale of the dynamics, but a completely inverted picture.

These questions are interesting and it is remarkable that they evolved from, in some sense, such a 'simple' system. However, I've completely exhausted myself by this point and currently lack the willpower to pursue these topics. I will end here, but most likely give some thought to this problem in the future.

Thank you very much for reading.

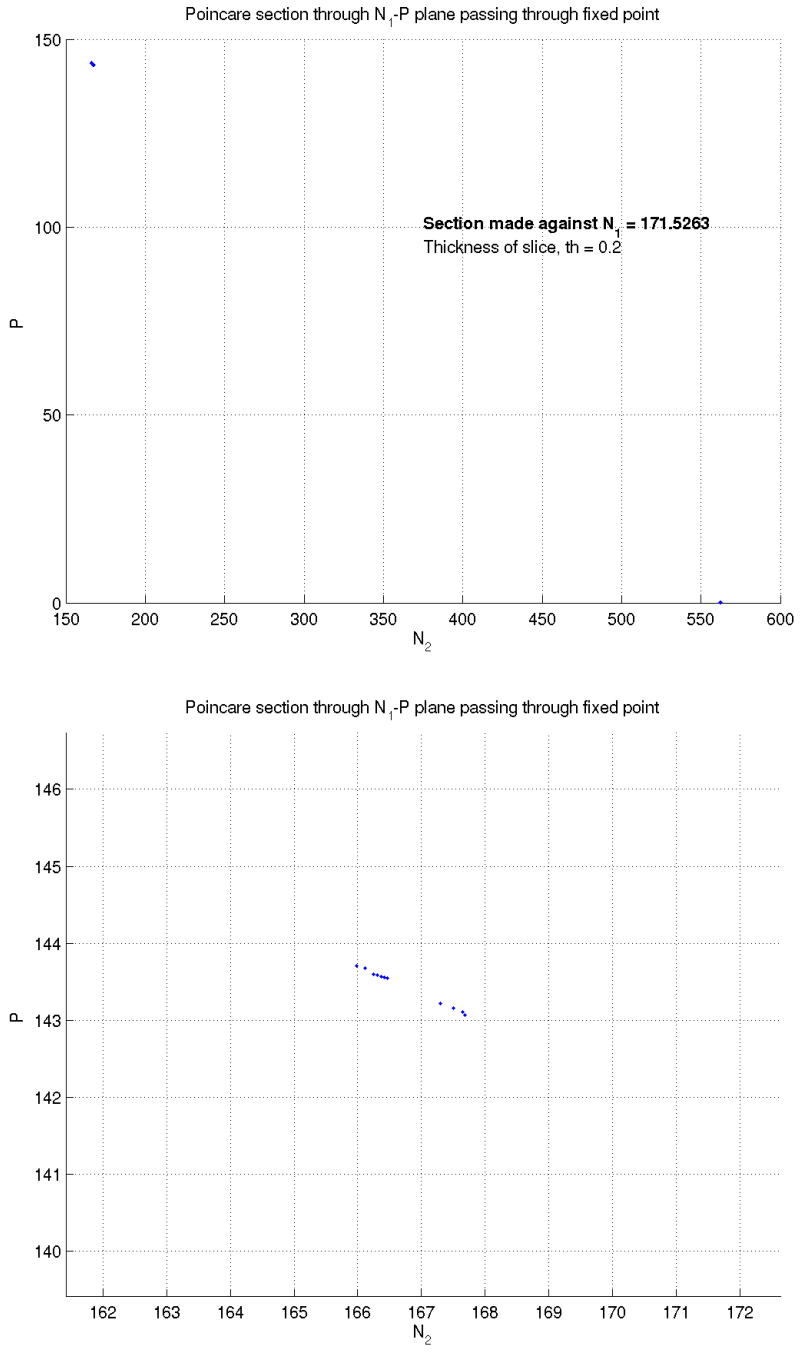

Figure 10: Poincaré section with the plane $N_1 = N_1^*$. (Above figure) The two main cuts arising from the limit cycle are evident. (Bottom figure) A magnified view of the 'point' on the upper left actually reveals two *distinct* passes through the slice. In interpreting the sections of this attractor, I generally had to focus on the top left slice (in this case approximately (160,145)) because the trajectories at the other end are much more compressed. This will be more apparent in the phase space representations of the attractor.

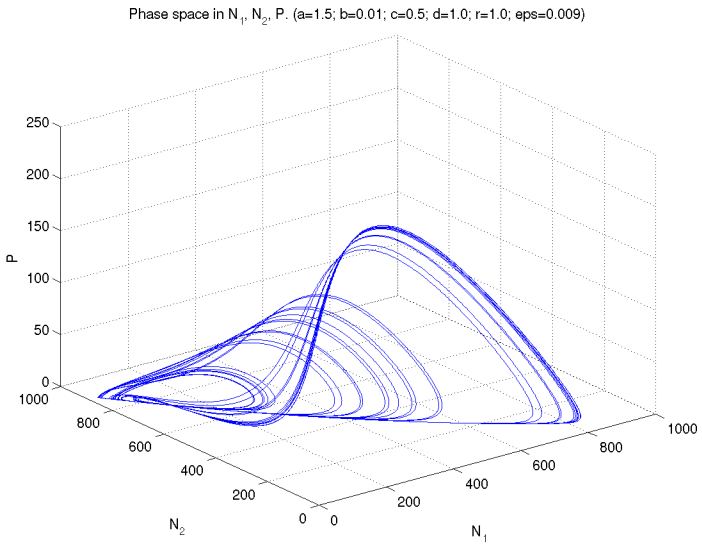

Figure 11: The chaotic attractor that develops through period doubling. ($k = 925$)

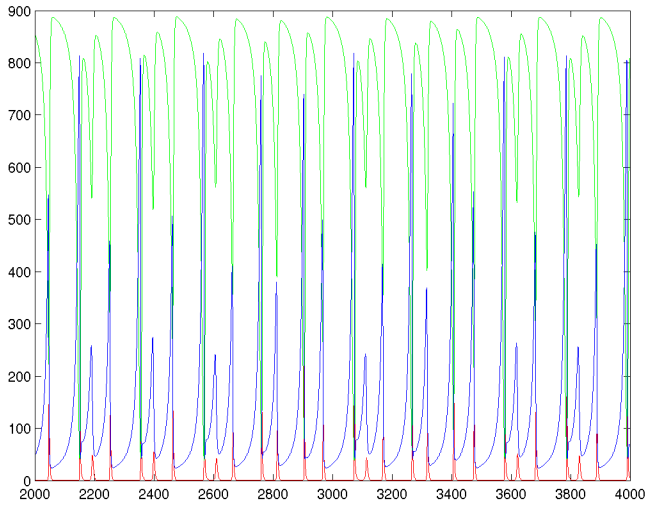

Figure 12: The superposition of the steady-state time series for N_1 (blue), N_2 (green) and P (red).

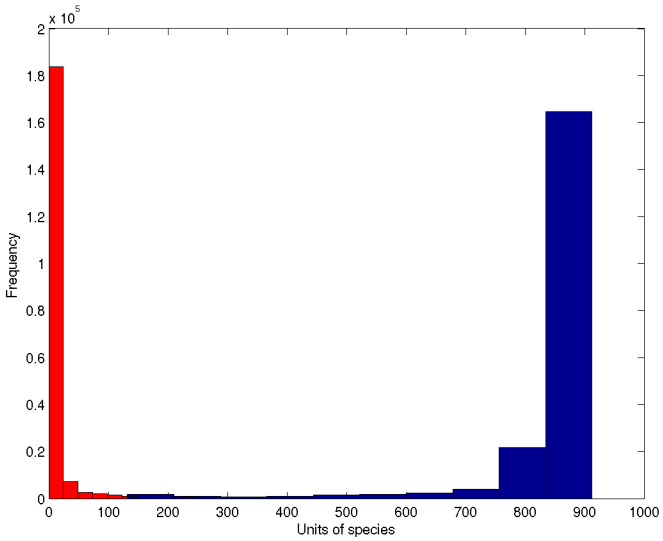

Figure 13: Statistical distribution of the prey populations $N_1(t) + N_2(t)$ (blue) and $P(t)$ (red). The predator population generally pales in comparison to the size of the prey population.

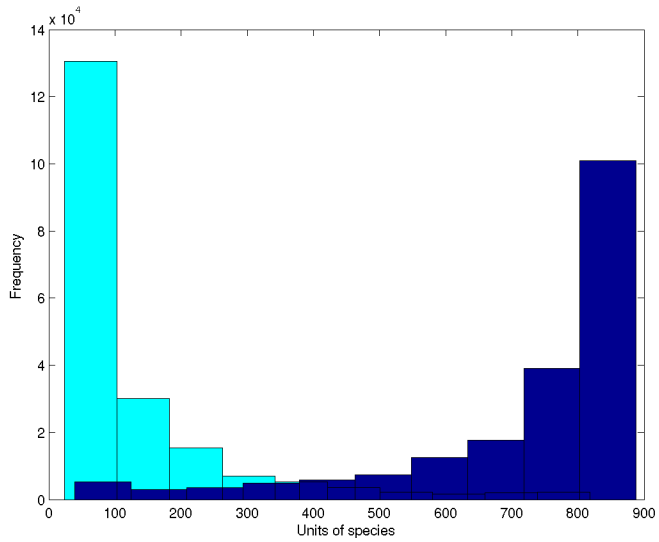

Figure 14: Statistical distribution of the prey populations $N_1(t)$ (cyan) and $N_2(t)$ (blue). The histogram reveals definite preference for N_2 in this system.

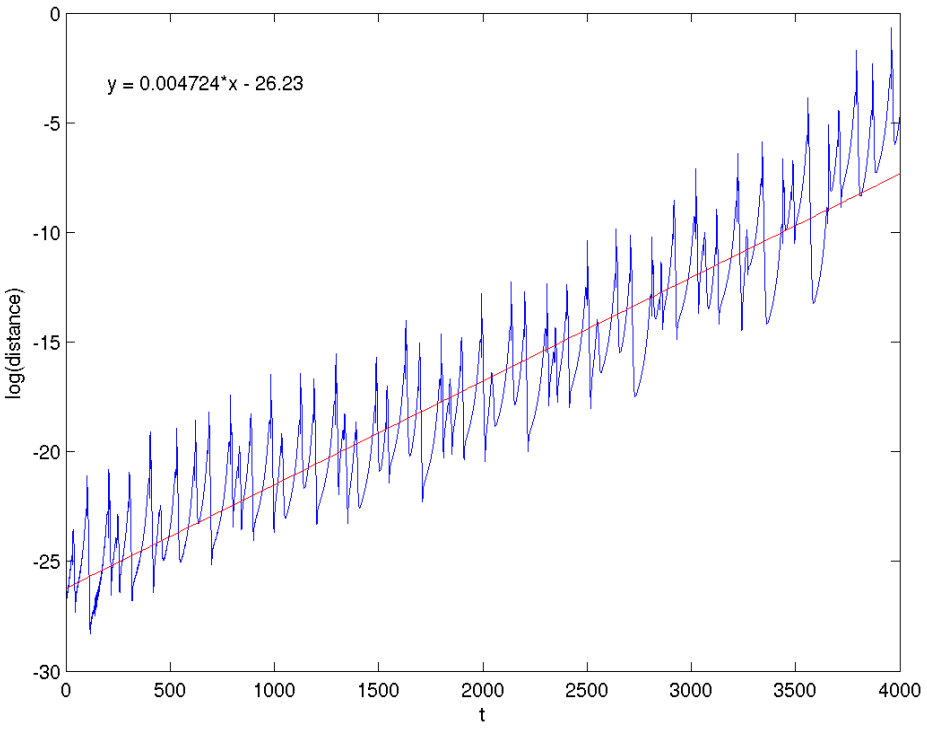

Figure 15: Calculation of the Lyapunov exponent using two nearby trajectories ($k = 925$).

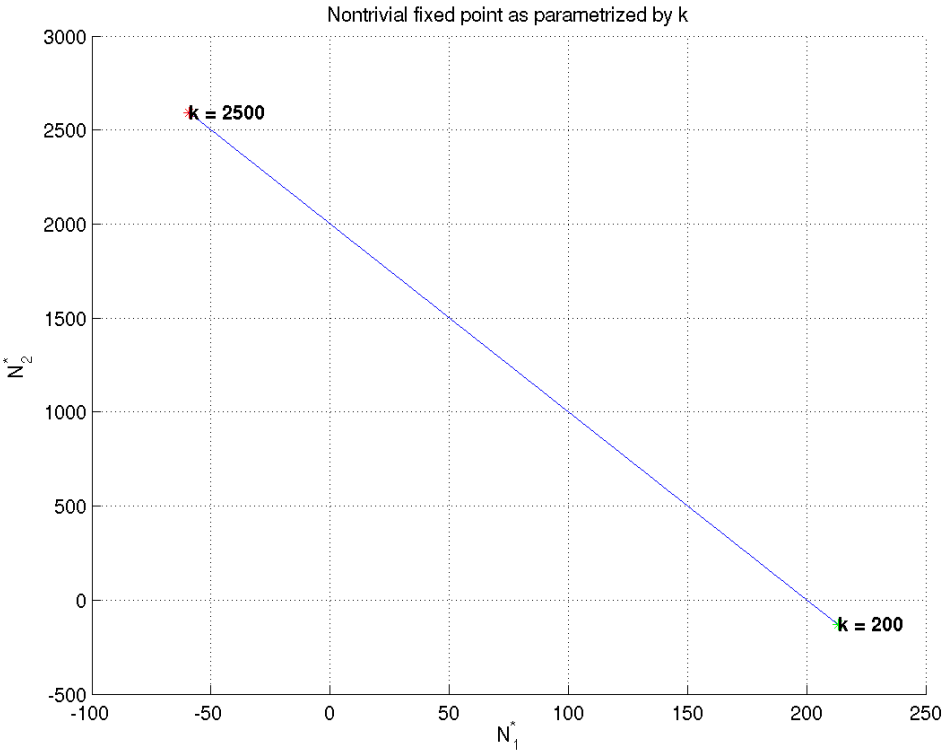

Figure 16: Projection of $(N_1, N_2, P)^* = \vec{f}(k)$ on the (N_1, N_2) plane. Large values of k tend to shift the fixed point in favor of N_2 at the expense of N_1.

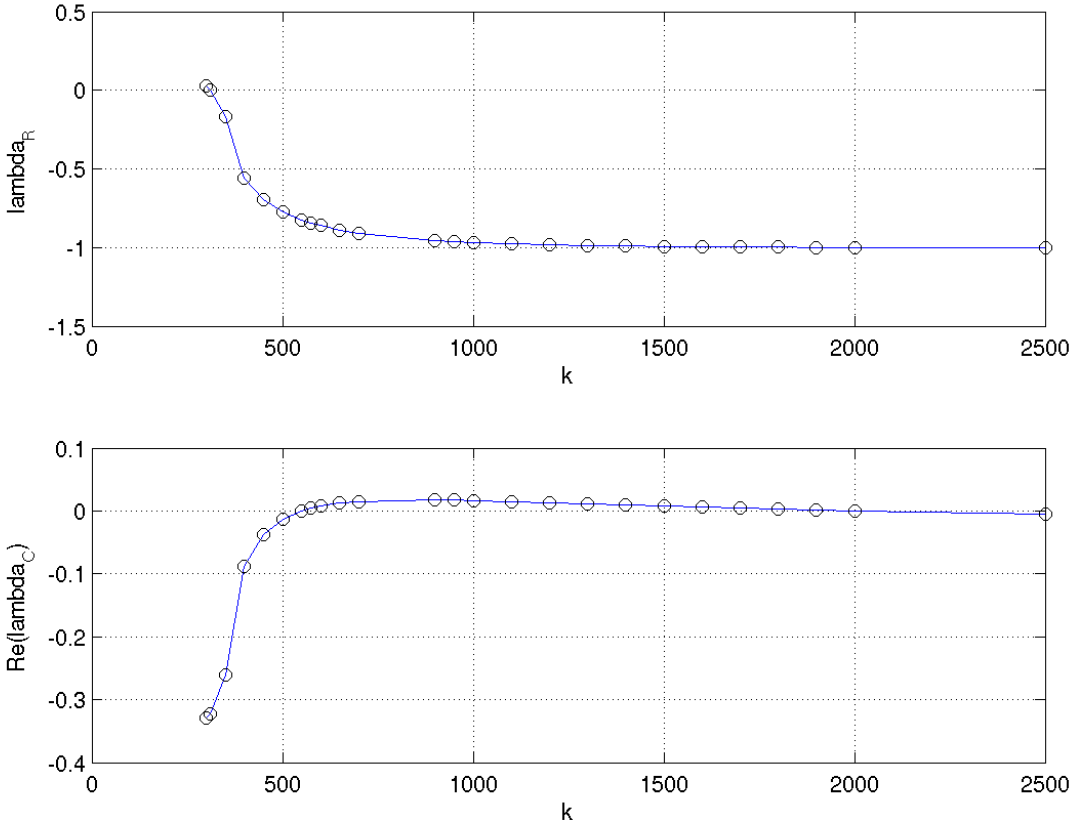

Figure 17: λ_R and $Re(\lambda_C)$ over a wide range of k.

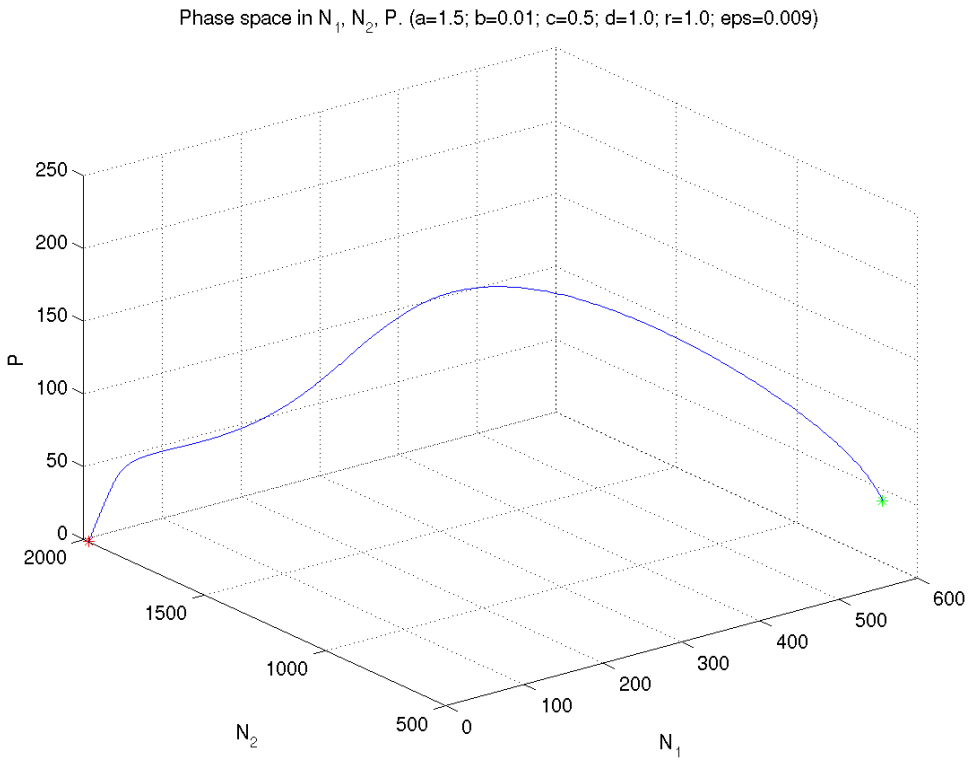

Figure 18: Evolution of the system from $(N_1, N_2, P)_0 = (580, 580, 50)$ at $k = 1980$. For all intents and purposes, the flow appears to approach a fixed point near the N_2 axis. This can be further verified by an analysis of the time series.